Supplementary Information

Simultaneous visualization of the extracellular and cytoplasmic domains of the epidermal growth factor receptor

Li-Zhi Mi, Chafen Lu, Zongli Li, Noritaka Nishida, Thomas Walz, and Timothy A. Springer

Nature Structural & Molecular Biology: doi:10.1038/nsmb.2092

Supplementary Fig. 1 Monomeric EGFR

a

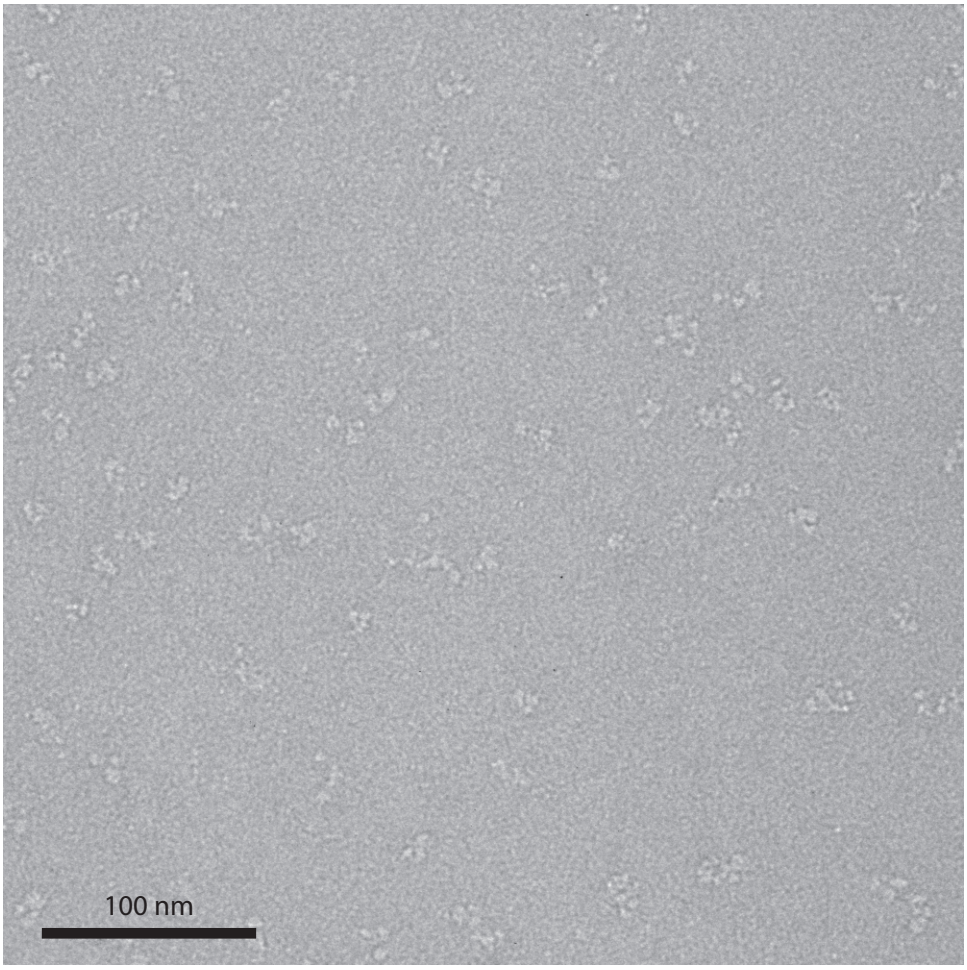

b 4,221 particles in 50 classes

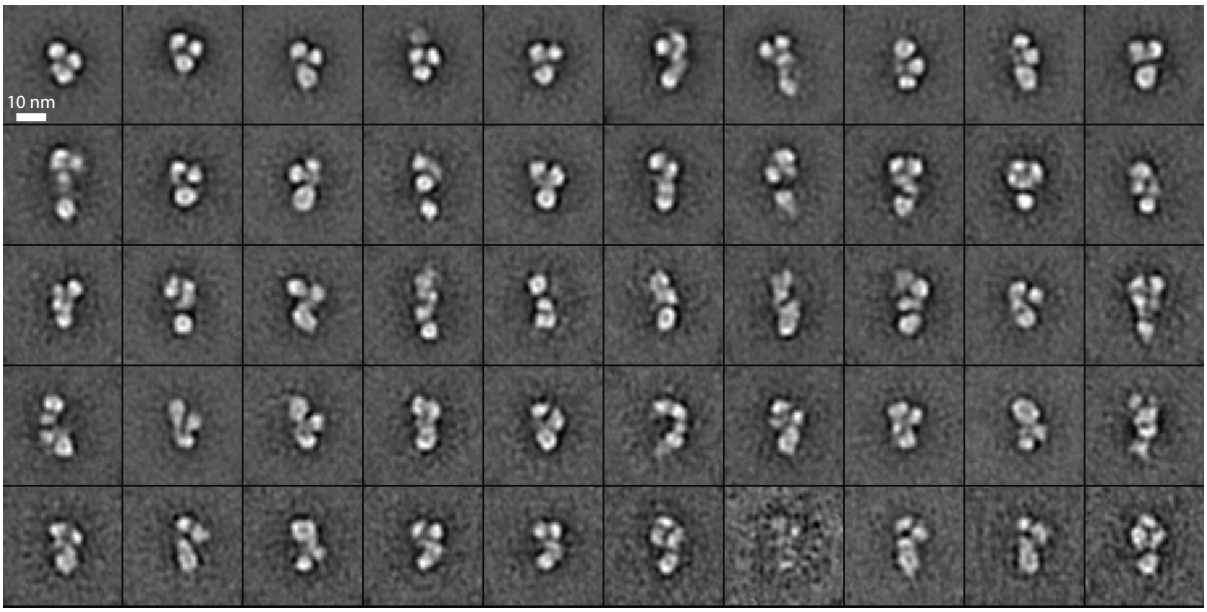

Supplementary Fig. 1. The unliganded EGFR. Representative electron micrograph field (a) and class averages (b). Averages are ranked (left to right in each row, from top to bottom row) by numbers of particles in each class.

Supplementary Fig. 2 Dimeric EGFR + EGF

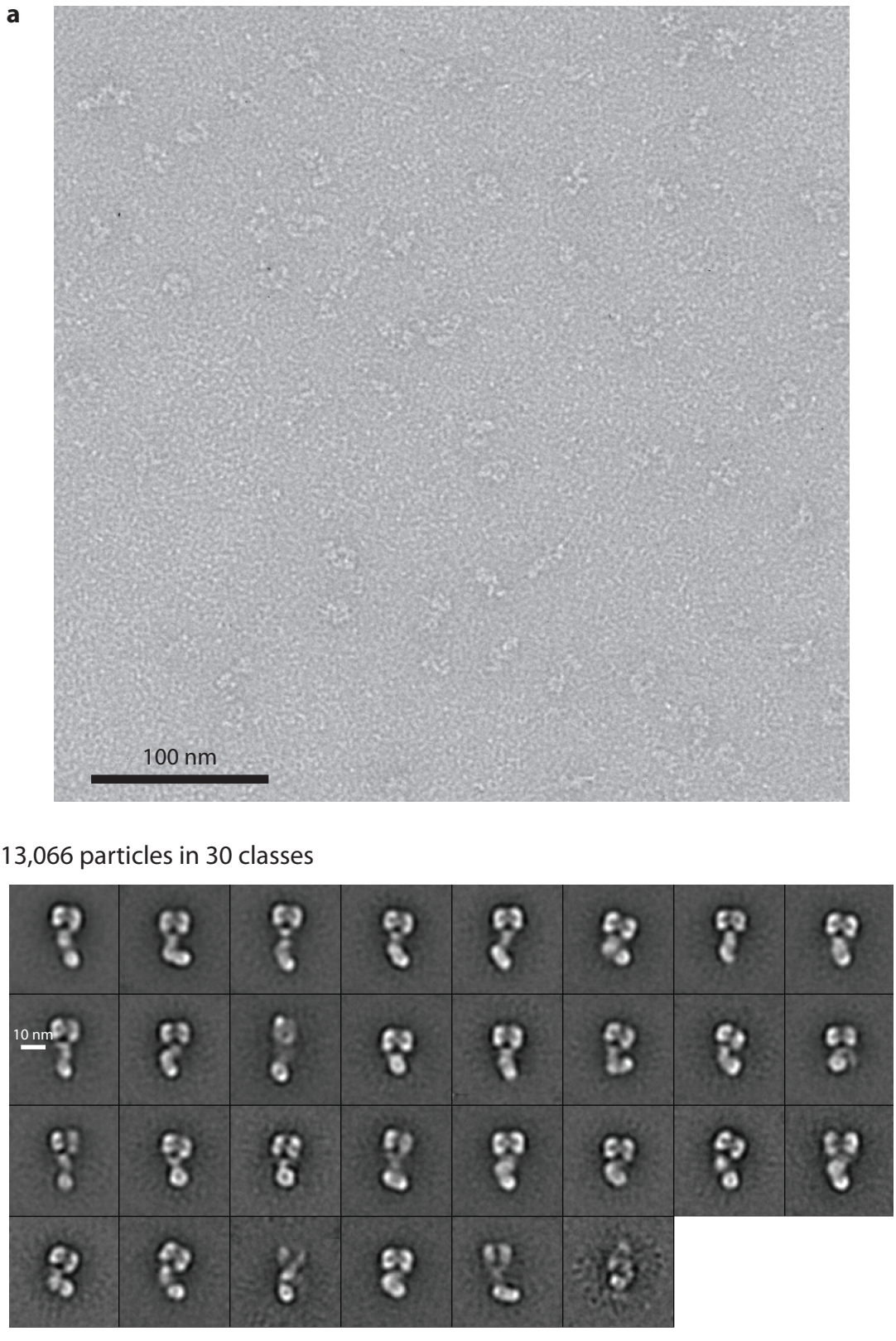

Supplementary Fig. 2. The EGFR in complex with EGF. Representative micrograph area (a), and class averages (b). Averages are ranked (left to right in each row, from top to bottom row) by numbers of particles in each class.

Supplementary Fig. 3 Dimeric EGFR V924R + EGF

a

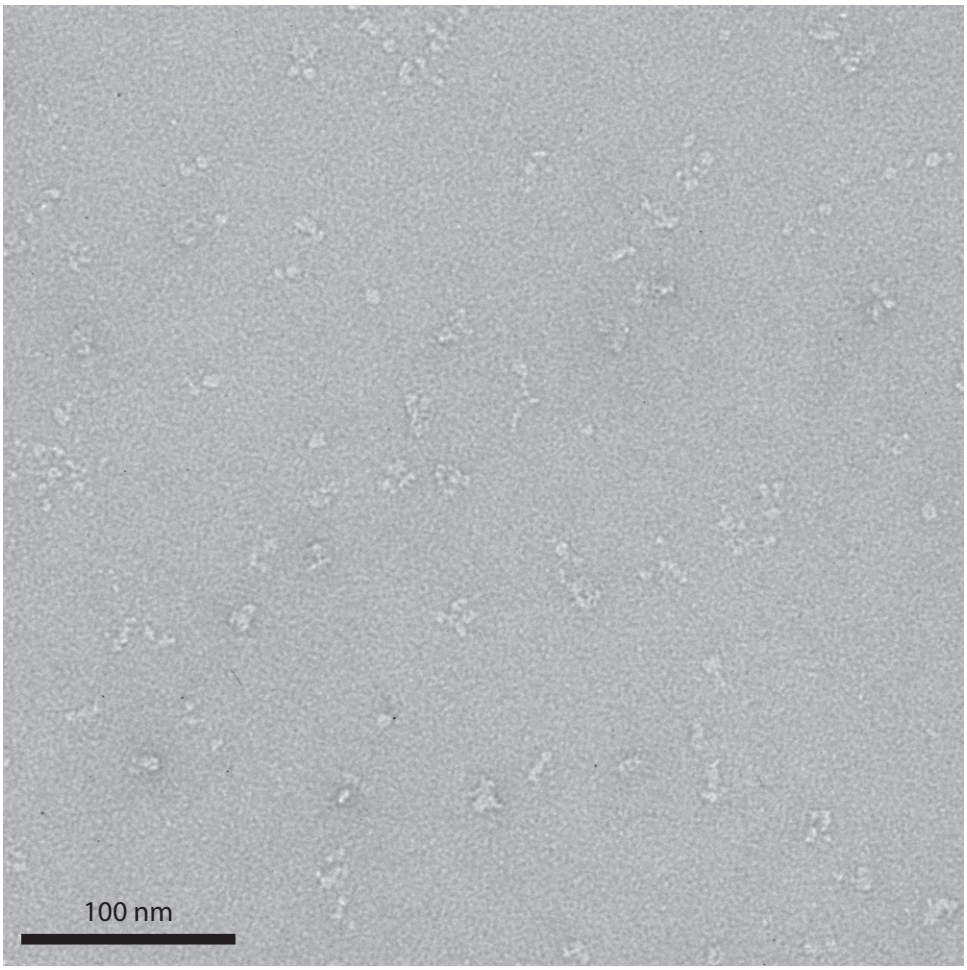

b 3,146 particles in 50 classes

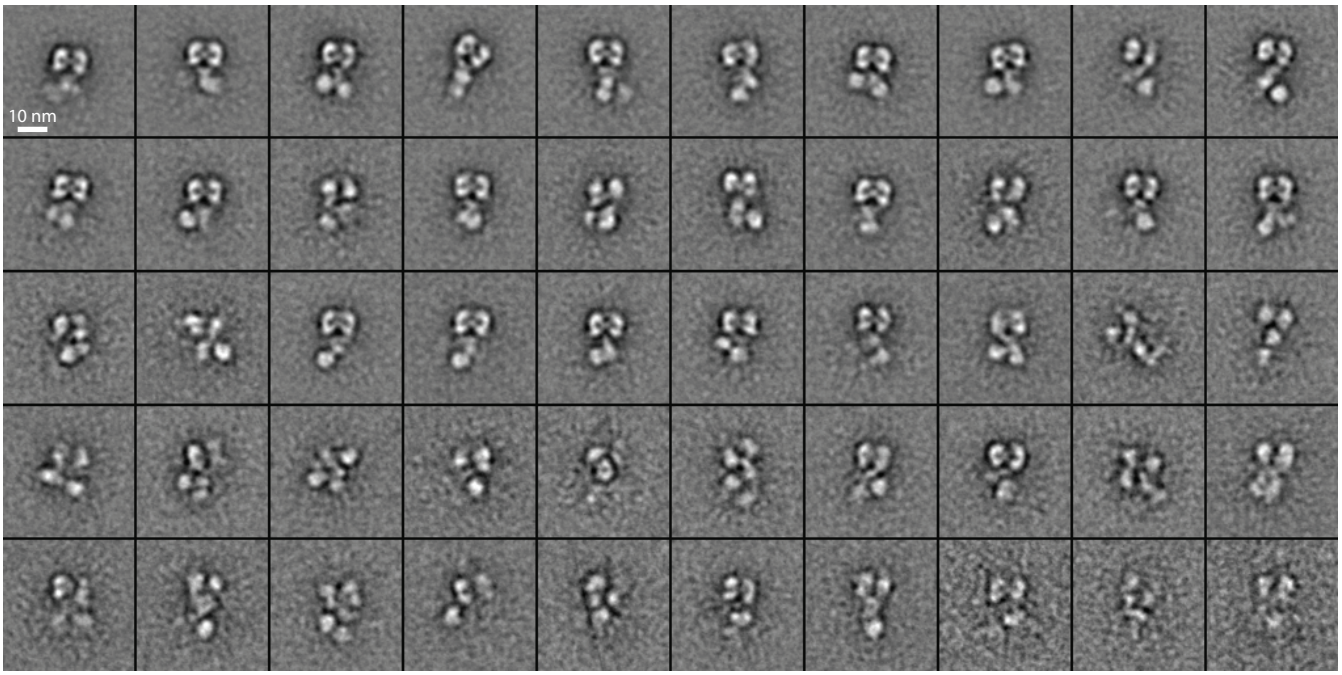

Supplementary Fig. 3. The EGFR V924R mutant. Representative micrograph area (a), and class averages (b). Averages are ranked (left to right in each row, from top to bottom row) by numbers of particles in each class.

Supplementary Fig. 4 Dimeric EGFR T669D S671D + EGF

a

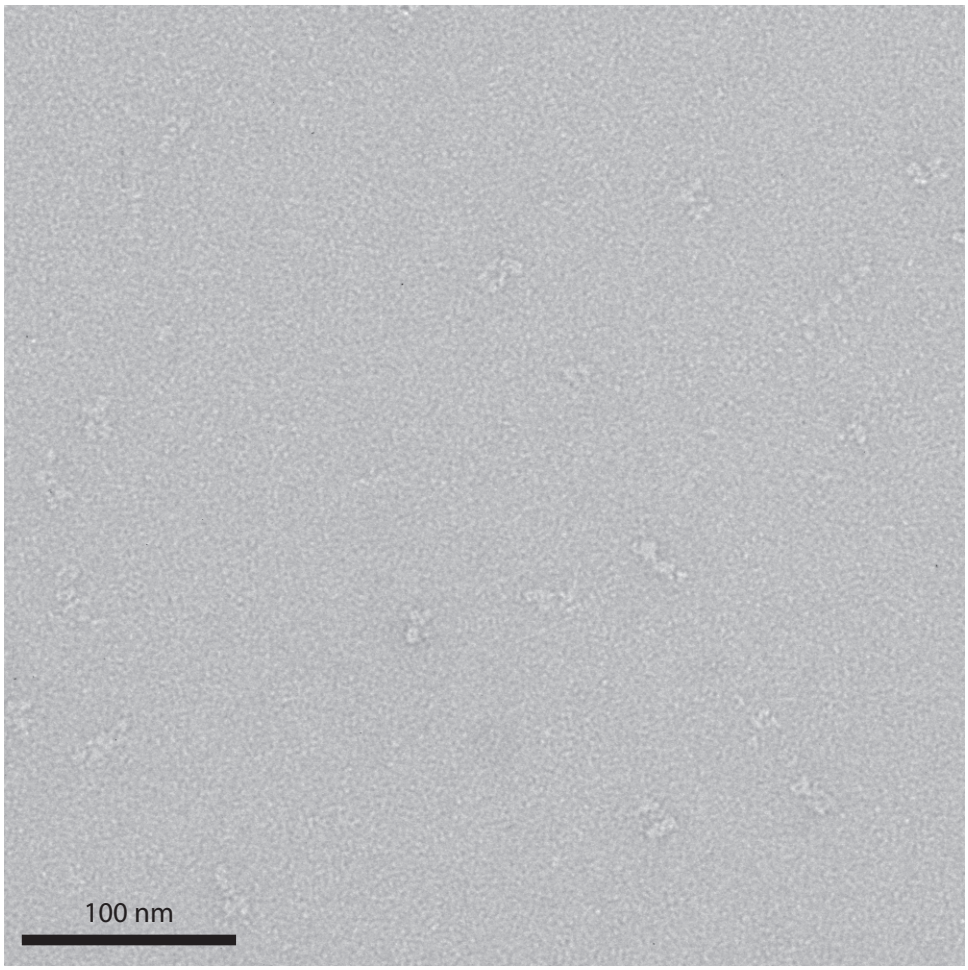

b 6,049 particles in 50 classes

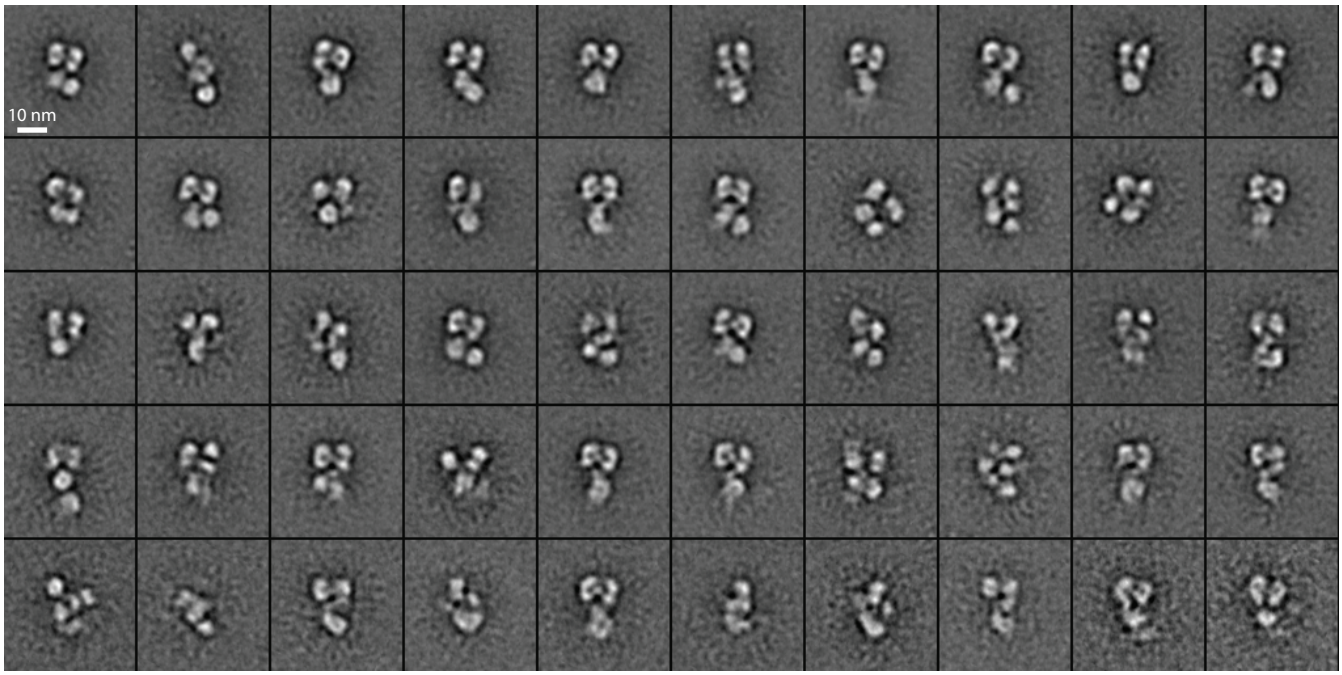

Supplementary Fig. 4. The EGFR T669D/S671D mutant. Representative micrograph area (a), and class averages (b). Averages are ranked (left to right in each row, from top to bottom row) by numbers of particles in each class.

Supplementary Fig. 5 Dimeric EGFR T654D + EGF

a

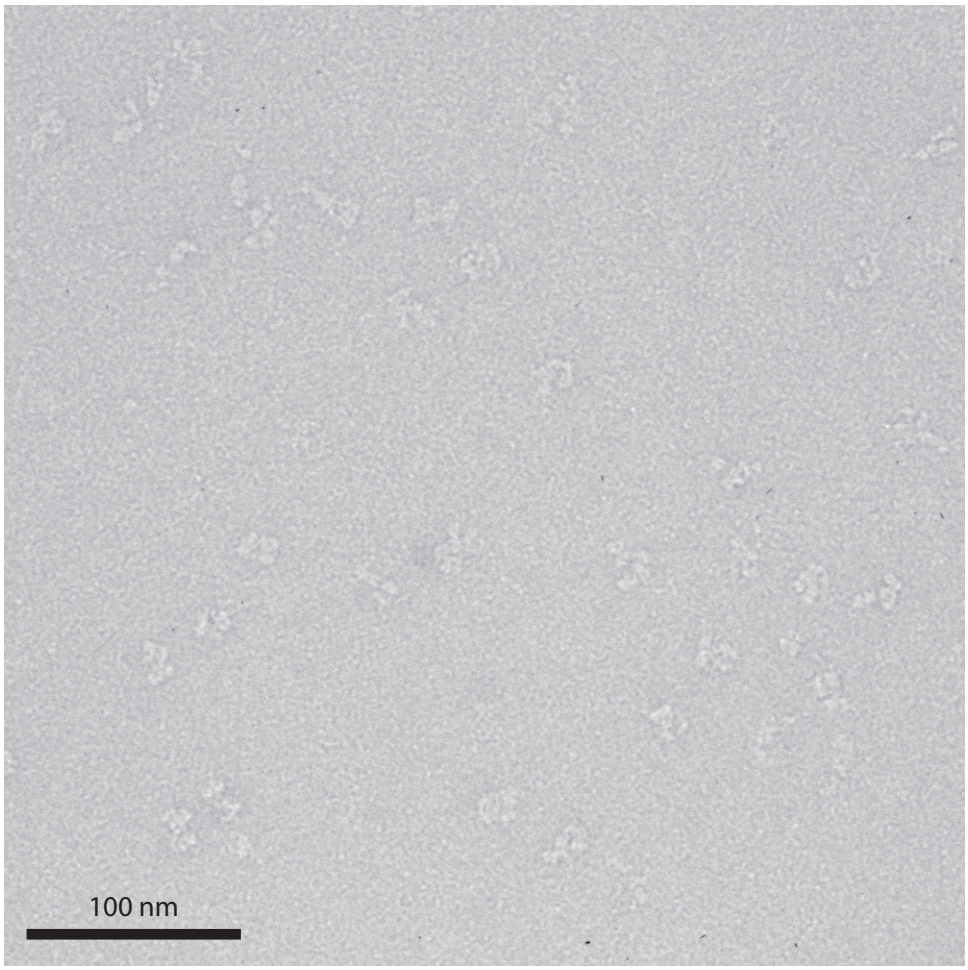

b 6,412 particles in 50 classes

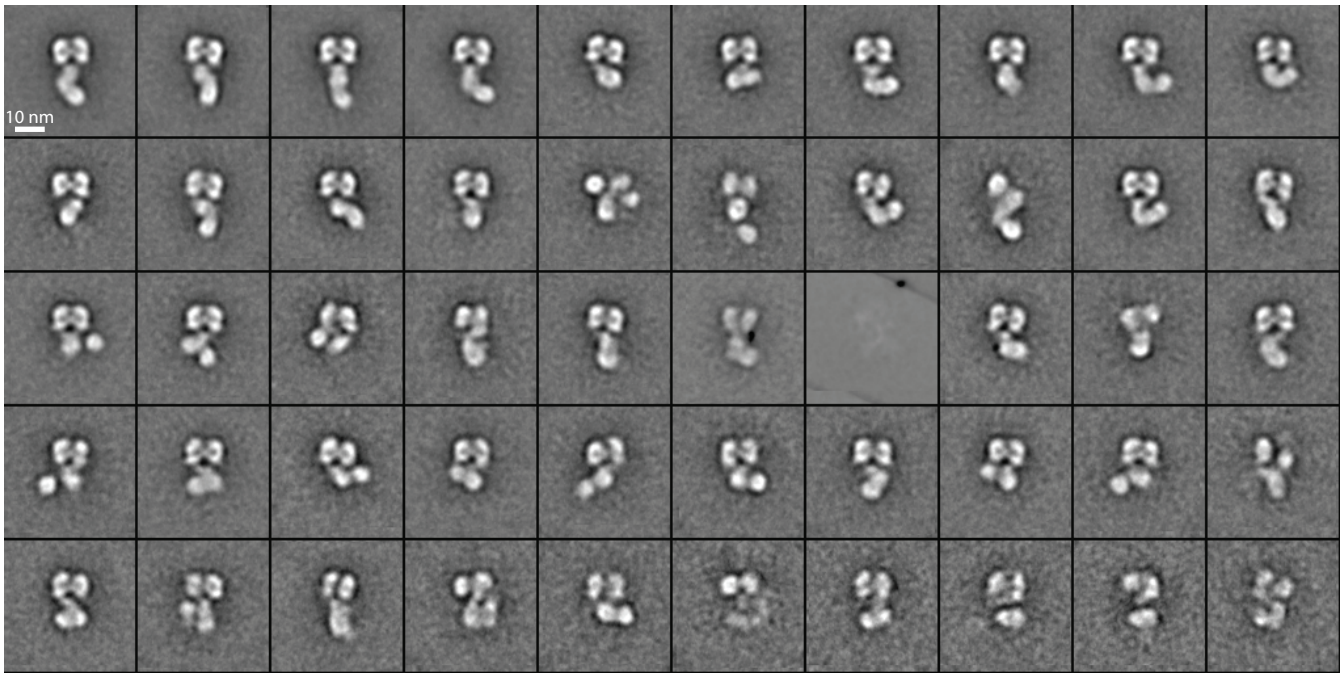

Supplementary Fig. 5. The EGFR T654D mutant. Representative micrograph area (a), and class averages (b). Averages are ranked (left to right in each row, from top to bottom row) by numbers of particles in each class.

Supplementary Fig. 6 Dimeric EGFR + EGF + Gefitinib

a

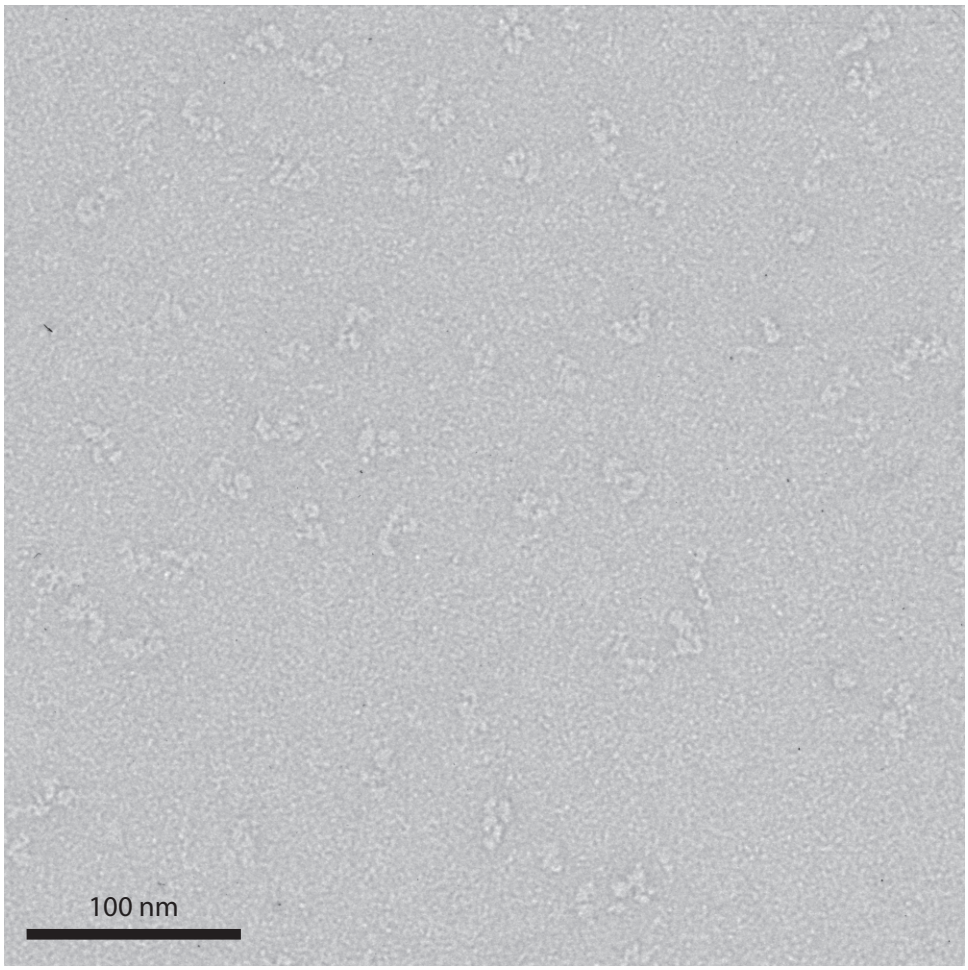

b 7,860 particles in 50 classes

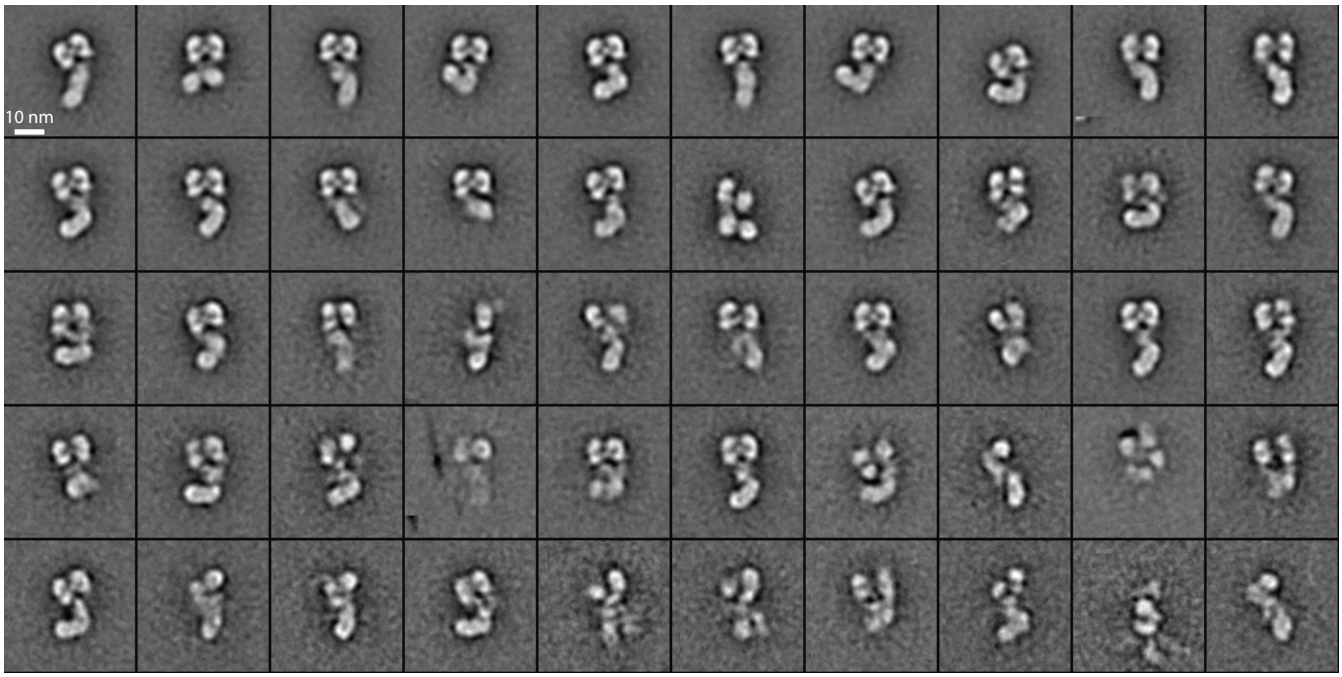

Supplementary Fig. 6. The EGFR in complex with EGF and Gefitinib. Representative micrograph area (a), and class averages (b). Averages are ranked (left to right in each row, from top to bottom row) by numbers of particles in each class.

Nature Structural & Molecular Biology: doi:10.1038/nsmb.2092

Supplementary Fig. 7 Dimeric EGFR + EGF + PD168393

a

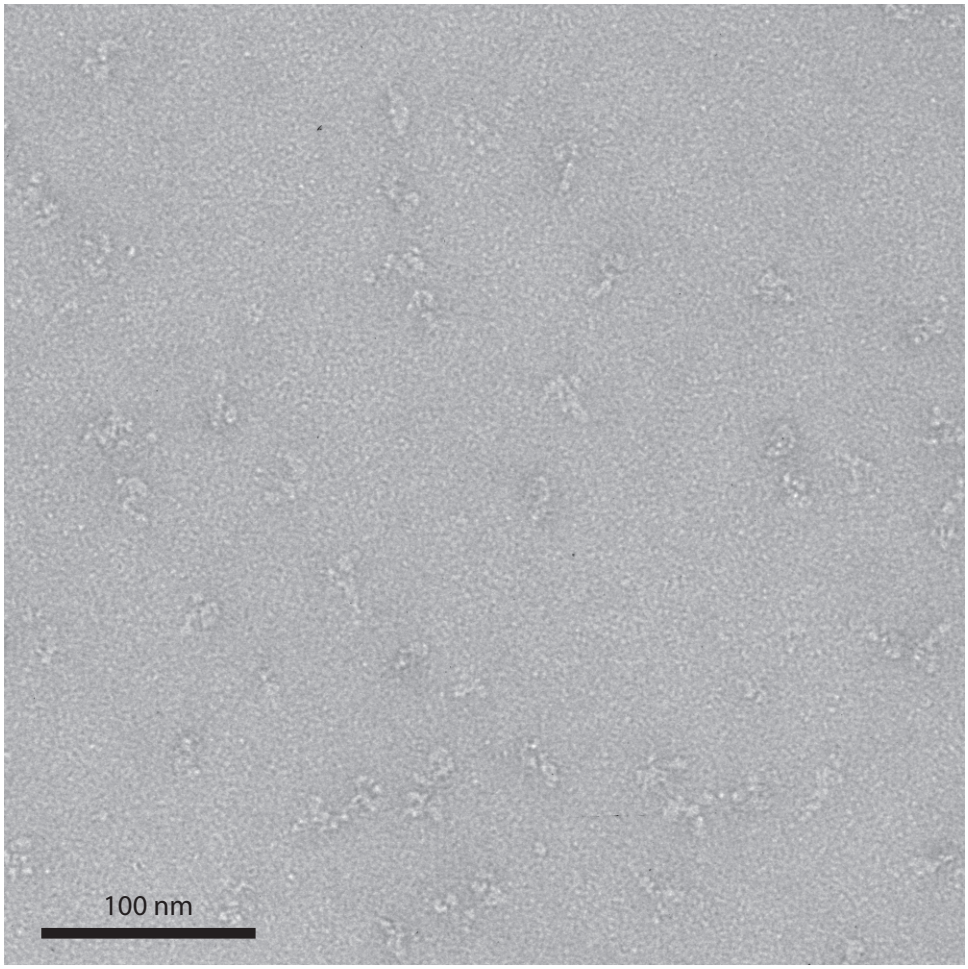

b 4,214 particles in 50 classes

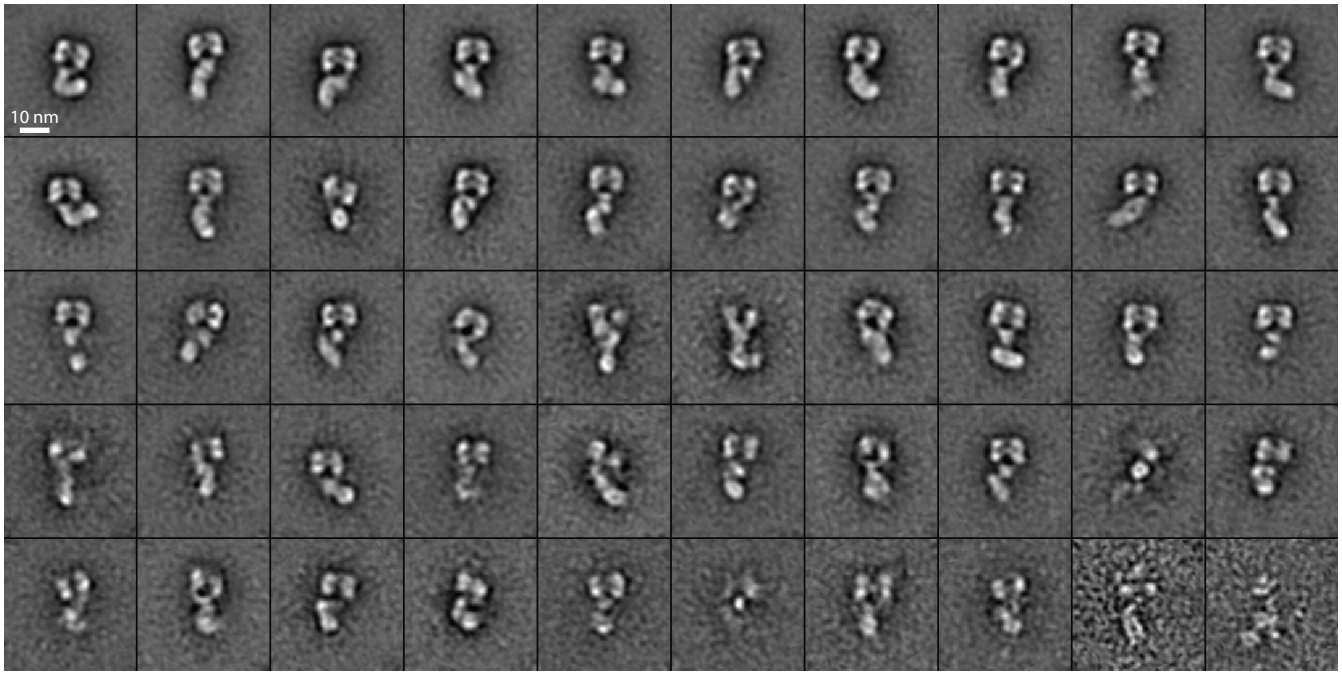

Supplementary Fig. 7. The EGFR in complex with EGF and PD168393. Representative micrograph area (a), and class averages (b). Averages are ranked (left to right in each row, from top to bottom row) by numbers of particles in each class.

Nature Structural & Molecular Biology: doi:10.1038/nsmb.2092

Supplementary Fig. 8 Dimeric EGFR + EGF + Lapatinib

a

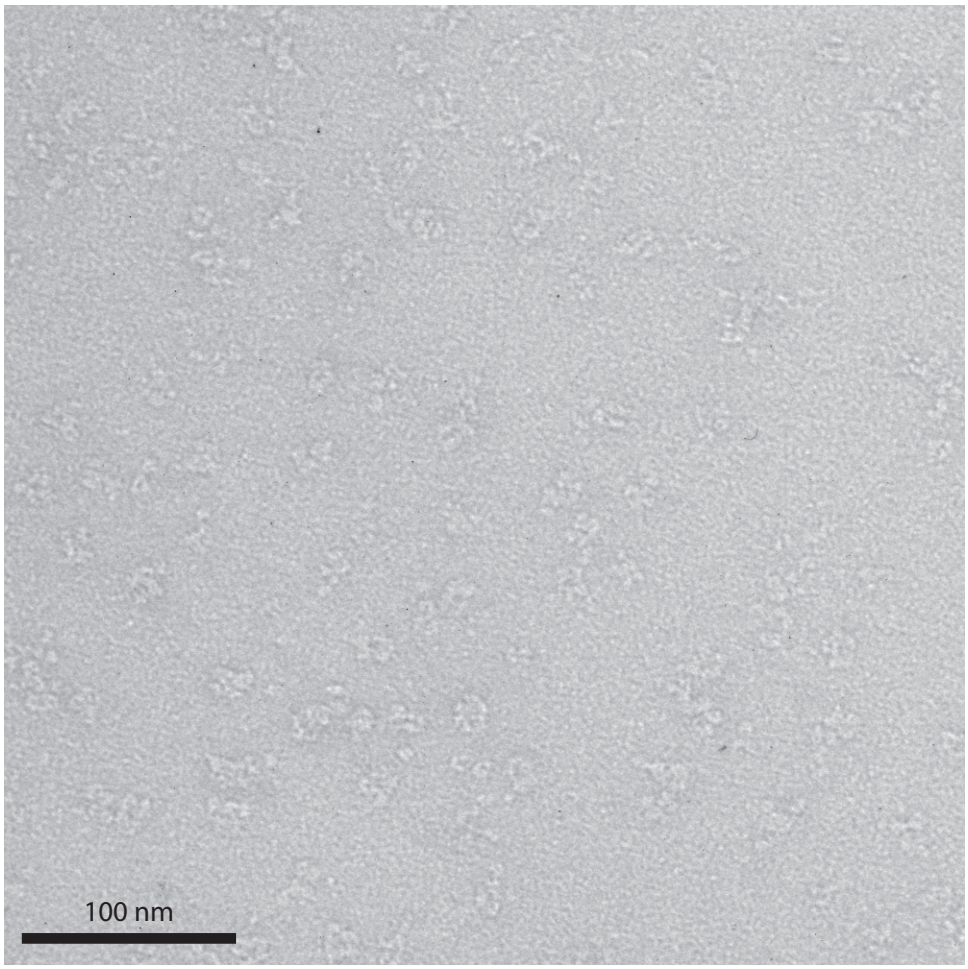

b 4,123 particles in 50 classes

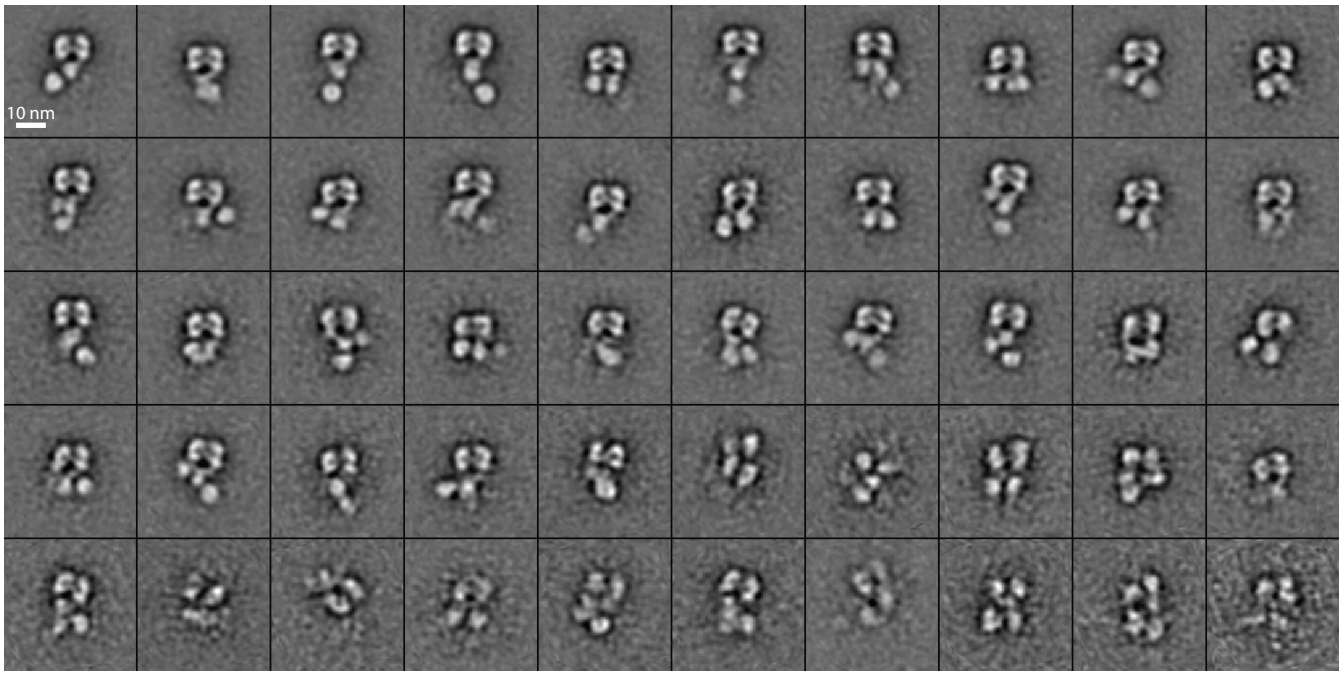

Supplementary Fig. 8. The EGFR in complex with EGF and lapatinib. Representative micrograph area (a), and class averages (b). Averages are ranked (left to right in each row, from top to bottom row) by numbers of particles in each class.

Nature Structural & Molecular Biology: doi:10.1038/nsmb.2092

Supplementary Fig. 9 Dimeric EGFR + EGF + HKI-272

a

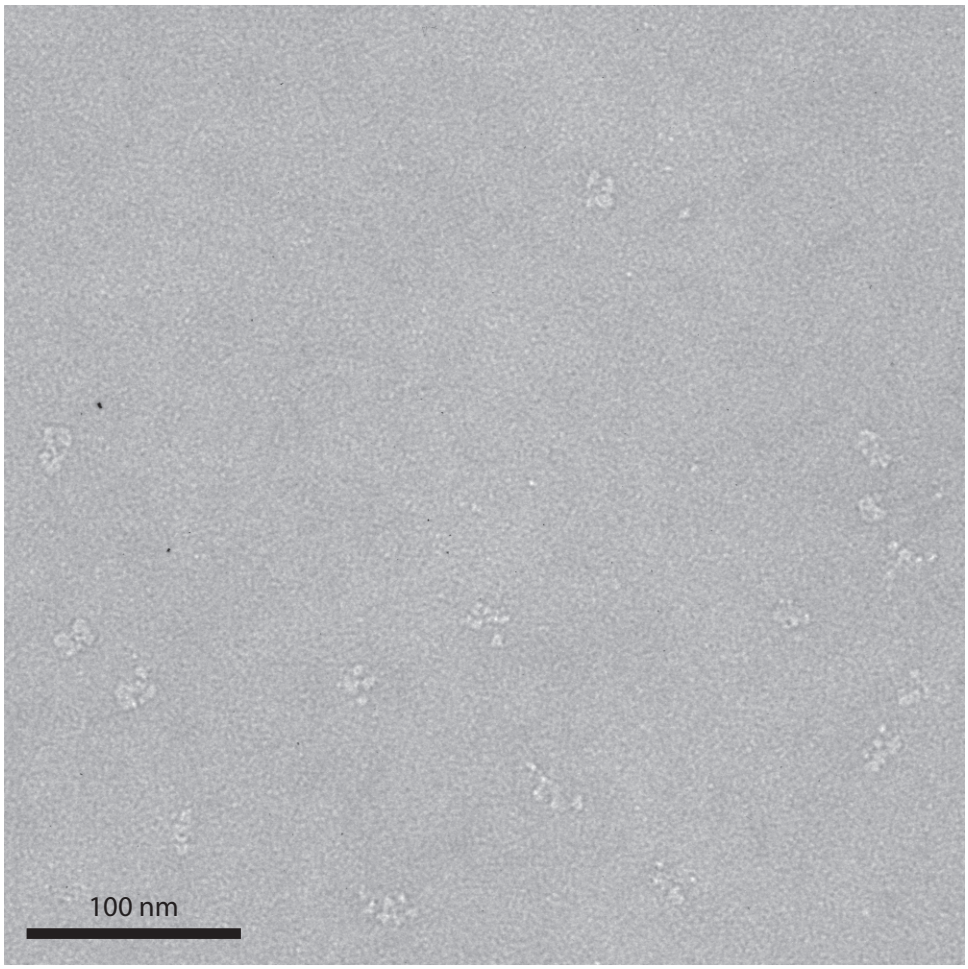

b 4,536 particles in 50 classes

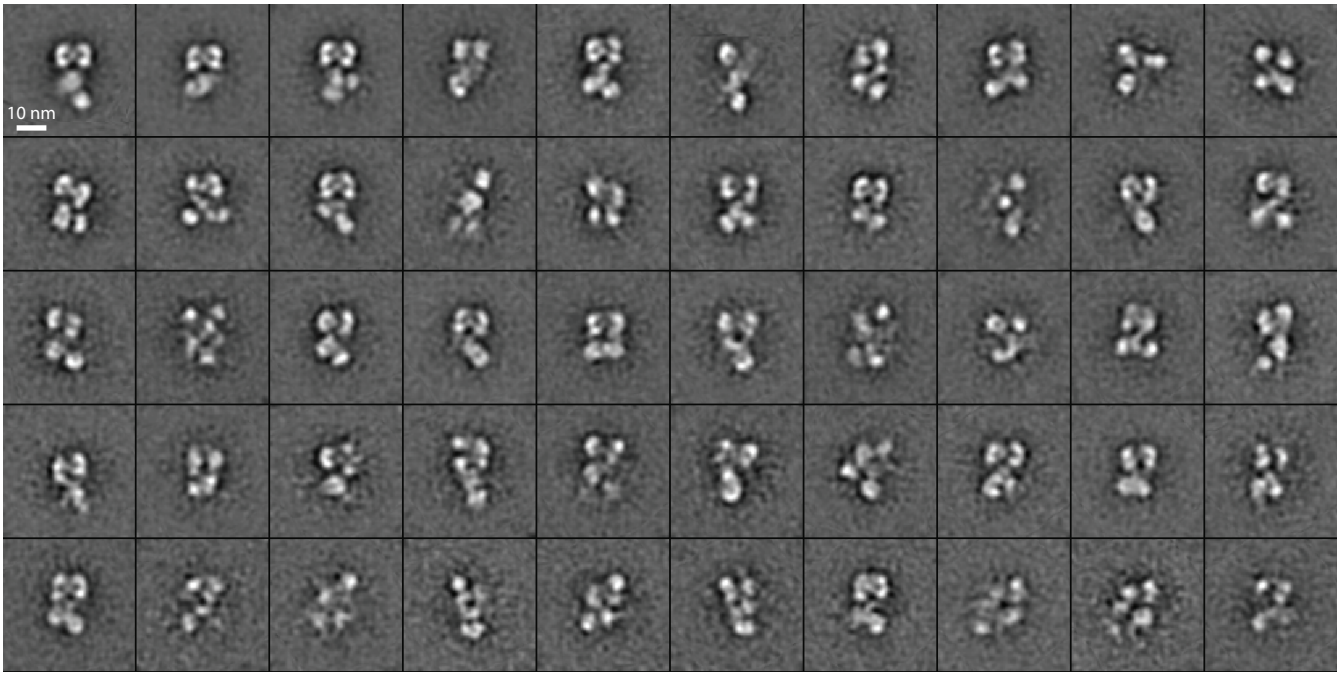

Supplementary Fig. 9. The EGFR in complex with EGF and HKI-272. Representative micrograph area (a), and class averages (b). Averages are ranked (left to right in each row, from top to bottom row) by numbers of particles in each class.

Nature Structural & Molecular Biology: doi:10.1038/nsmb.2092

Supplementary Fig. 10 Monomeric EGFR

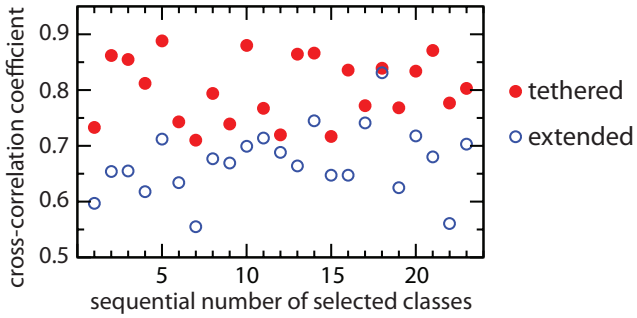

Supplementary Fig. 10. Correlation of monomeric EGFR ectodomain density with different ectodomain crystal structures. Twenty-three class-averages of monomeric EGFR had space between the extracellular and intracellular domains. Their ectodomain densities all cross-correlated better with projections from the monomeric tethered (red) than a monomer from the extended, dimeric crystal structure (blue).

Supplementary Fig. 11

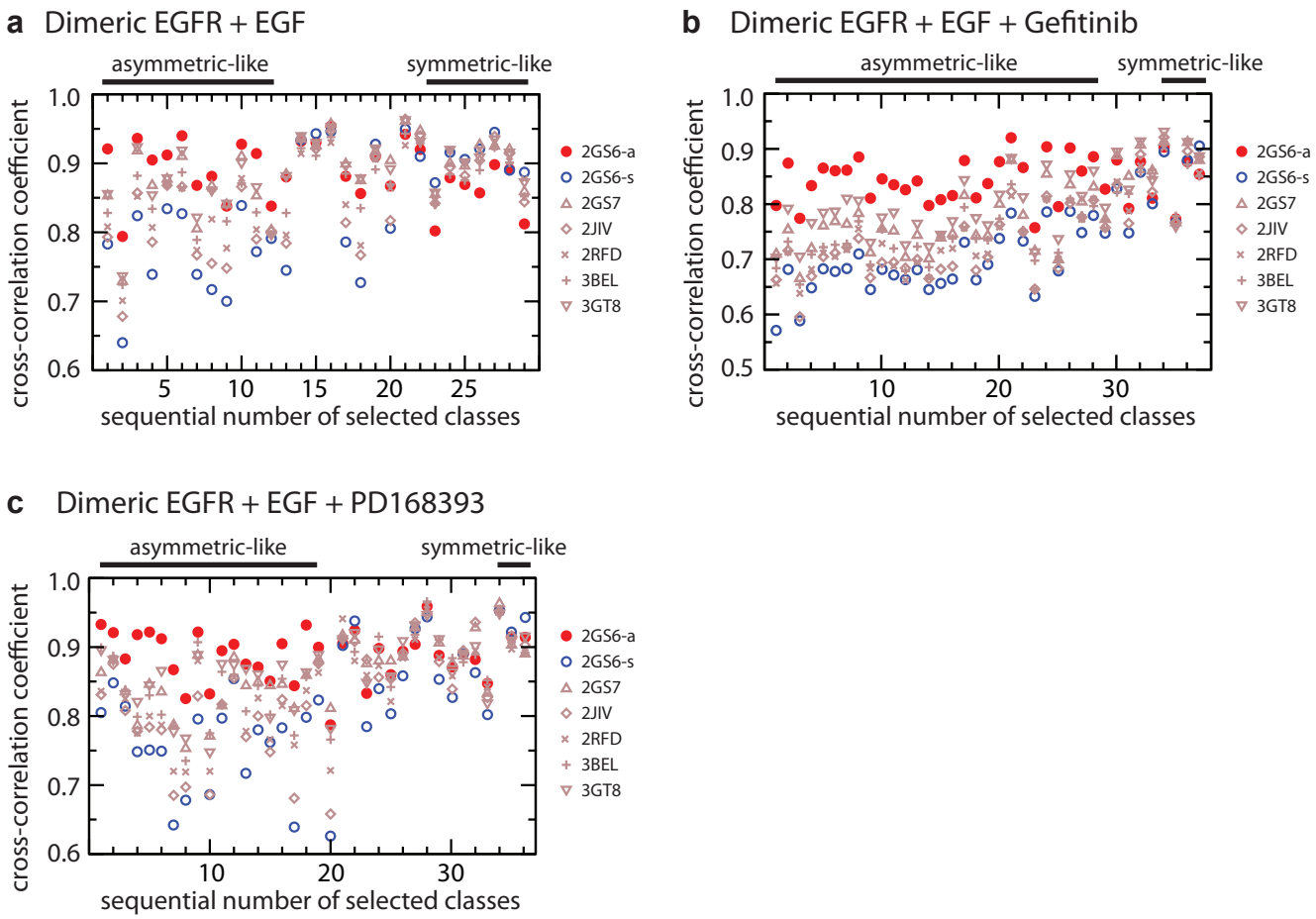

Supplementary Fig. 11. Correlation of the intracellular densities of liganded receptors with different crystallographic kinase dimer structures. A. complex with EGF. The intracellular domain densities from twenty-nine class averages of EGF-bound receptors were cross-correlated with projections from different crystallographic kinase dimers. Twelve that visually resembled the asymmetric, rod-like dimer (overlined) correlated best with the asymmetric kinase dimer. Seven that visually were ring-like and globular (overlined) correlated better with symmetric dimers. B. Complex with EGF and gefitinib. The intracellular domain densities from thirty-seven class averages of EGFR complexes were cross-correlated with projections from different crystallographic kinase dimers. Twenty-eight that visually resembled the asymmetric, rod-like dimer (overlined) correlated best with the asymmetric kinase dimer. Four that visually were ring-like and globular (overlined) correlated better with symmetric dimers. C. Complex with EGF and PD168393. The intracellular domain densities from thirty-six class averages of EGFR complexes were cross-correlated with projections from different crystallographic kinase dimers. Nineteen that visually resembled the asymmetric, rod-like dimer (overlined) correlated best with the asymmetric kinase dimer. Three that visually were ring-like and globular (overlined) correlated better with symmetric dimers.

Supplementary Fig. 12

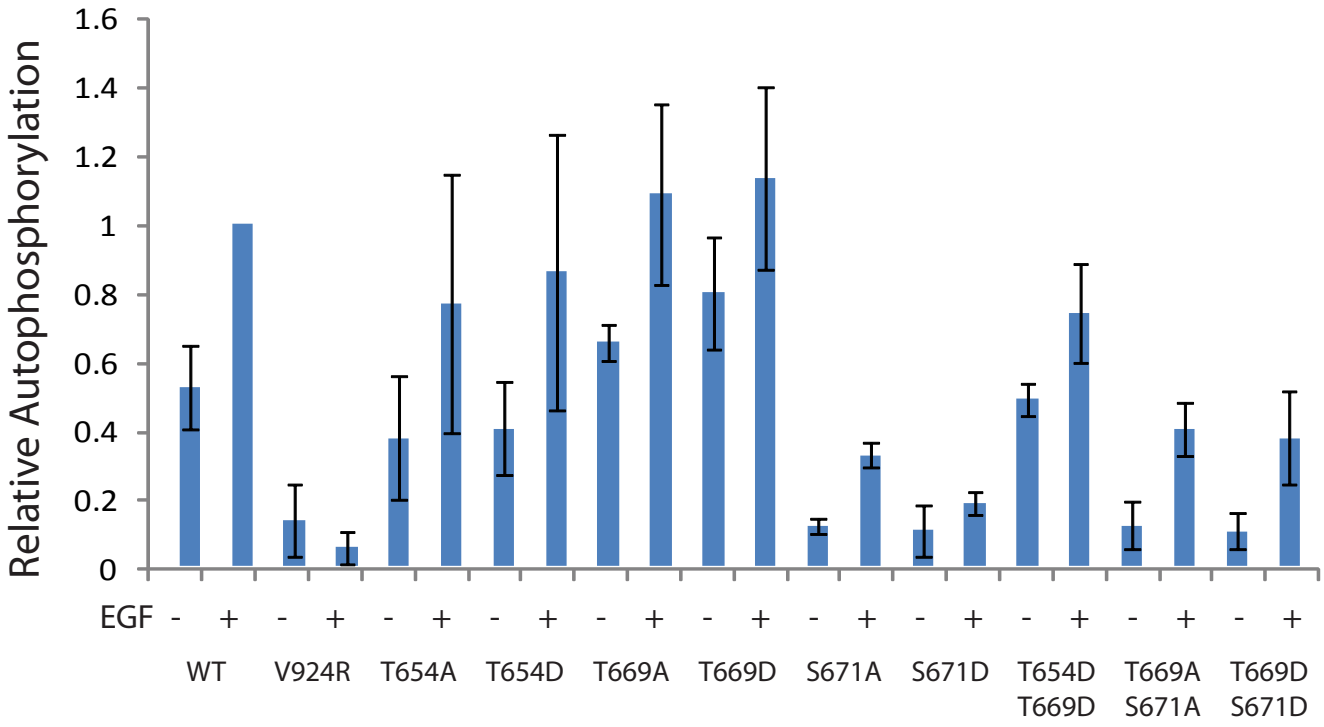

Supplementary Fig. 12. Kinase activities of EGFR juxtamembrane mutants. Transiently transfected 293T cells were treated with or without EGF and subjected to Western blotting with protein C antibody to a C-terminal tag and 4G10 antibody to phosphotyrosine. Each mutant was tested in two independent experiments in duplicate. The ratio of 4G10 and protein C antibody chemiluminescence was calculated relative to wild-type, EGF-treated receptor. Relative autophosphorylation and s.d. of four measurements are shown.